

Received September 16, 2018, accepted October 3, 2018, date of publication October 9, 2018, date of current version October 31, 2018.

Digital Object Identifier 10.1109/ACCESS.2018.2874980

Blind Deconvolution for Image Deblurring Based on Edge Enhancement and Noise Suppression

CHENGTAO CAI, HAIYANG MENG^{ID}, AND QIDAN ZHU

College of Automation, Harbin Engineering University, Harbin 150001, China

Corresponding author: Haiyang Meng (menghaiyang@hrbeu.edu.cn)

This work was supported in part by the National Natural Science Foundation of China under Grant 61673129 and Grant 51674109, in part by the Fundamental Research Funds for the Central Universities under Grant HEUCF180405, and in part by the Harbin Application Research Funds under Grant 2016RQQXJ096.

ABSTRACT This paper denotes to obtain an accuracy blur kernel and a shape image. An efficient method that blind deconvolution for image deblurring based on edge enhancement and noise suppression is proposed. First, we exploited an edge detection method to extract the strong edge portion of blurred image. Then, the blurred image was divided into weak edge portion and strong edge portion. At this time, we apply a trilateral filter method to suppress the noise in the weak edge portion. Through mathematical operations for weak edge portion and strong edge portion, we can obtain the new blurred image which as the input of blur kernel estimation. At the phase of the kernel estimation, the problem can be solved via alternate between x and k updating. In addition, we utilize improved fast iterative shrinkage thresholding algorithm method to solve the optimization problem. Finally, non-blind deconvolution was employed at the phase of image recovery. A comprehensive evaluation shows that our approach achieves state-of-the-art results for uniformly blurred images.

INDEX TERMS Edge enhancement and noise suppression, trilateral filter, blur kernel estimation, blind deconvolution, IFISTA.

I. INTRODUCTION

Image deblurring has attracted considerable attention recently due to its involvement of many challenges in problem formulation, regularization, and optimization. Image blur often results from relative motion between a camera and the scene (e.g., camera shake) during the exposure time. It causes significant image degradation, especially in the low light conditions where longer exposure time is required. Although the blur effect may be reduced by setting a faster shutter speed, it inevitably generates significant amount of noise.

To handle image blur, a conventional blur model assumes a spatially invariant blur kernel [9]. For image blur problem, the model can be described as follows:

$$B = l \otimes k + n \quad (1)$$

where B and l are, respectively blurred image and latent image, k is the blur kernel (a.k.a. point spread function, PSF), n refers to an additive i.i.d. noise term sampled from an zero-mean Gaussian distribution [12]–[14], and \otimes denotes a convolution operator. Our goal is to exploit an available method to get a better approximate solution to get the best latent image l . According to (1), the most challenging

problem of image deblurring is the blur kernel estimation, which is related to the quality of restored image for the image deblurring. Obtaining a high quality image from a blurred image is the ultimate goal of all researchers in this field. Nevertheless, a precise blur kernel is the key to obtaining high quality images. Therefore, blur kernel estimation is the most important part of this literature.

Image deblurring can be categorized into two main approaches based on variational Bayesian inference, and Maximum a Posteriori (MAP) estimation. Fergus et al. presented an algorithm using a mixture of Gaussians to learn an image gradient prior via variational Bayesian inference [25] and Levin et al. also analyzed the method based on variational Bayesian inference [26]. However, the optimization process of variational Bayesian inference is computationally expensive. In recent years, MAP method, having been developed with different likelihood functions and image priors [8], is widely applied to image deblurring [27]–[30].

Many algorithms have been proposed in recent decades [2]–[6] in order to obtain the highly quality image based on MAP. Restoring blur kernel from a single image is a challenging task because a single image lacks a kernel

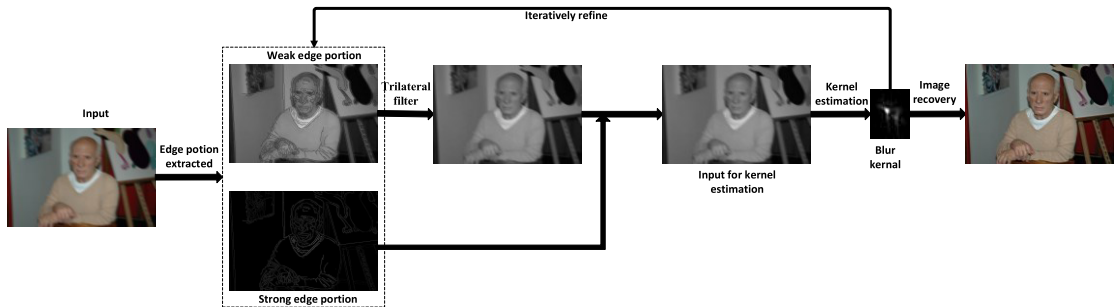


FIGURE 1. The proposed algorithm pipeline.

that contains ambiguous information. If one assumes that the blur kernel or point spread function (PSF) - is shift-invariant, image deconvolution can solve this problem well. Image deconvolution can be further separated into the blind and non-blind. In non-blind deconvolution, the motion blur kernel is assumed to be known or computed, such as the Richardson-Lucy (RL) and ForWaRD methods [11]; the only task remaining is to estimate the sharp latent image. In the case of blind deconvolution, the problem is even more ill-posed, since both the blur kernel and latent image are assumed unknown.

When the kernels are unknown, image deblurring is treated as a blind deconvolution problem. To solve the problem of blind deconvolution and obtain a high quality image, a majority of algorithms have been developed [15]–[18], Gong *et al.* [1] and Li *et al.* [10] proposed the promoting group sparsity to estimate blur kernel estimated the blur kernel by external patch priors. There are also many algorithms that improve the quality of image deblurring by improving the regularization term. ℓ_1 -norm [20]–[22] is often used on k to encourage the sparsity. Tikhonov regularization [23], [24] is a classical regularization algorithm that many algorithms are extended on it. This regularization method can prevent overfitting and enhances the non-convexity of the function.

In this paper, we proposed an efficient method that blind deconvolution for image deblurring based on edge enhancement and noise suppression. Since image edge information and noise suppression are critical to the estimation of blur kernel, this paper is dedicated to solving the problem of reducing the image noise and salient image edges enhancement to estimate the accuracy blur kernel. The proposed method can be mainly divided into three steps: edge enhancement and noise suppression, blur kernel estimation and image recovery. FIGURE.1 shows our algorithm pipeline.

Given a blurred image, we firstly exploited Sobel operator to get the strong edge portion and weak edge portion. For the weak edge portion, the trilateral filter was used to suppress the noise and enhance. This filter is improved based on bilateral filter. Not only does it suppress impulse noise well, but it also can sharpen image edge information. What's more, the method also can effectively restore images that are contaminated by Gaussian noise and impulse noise

simultaneously. Then, the input image of kernel estimation can be obtained by mathematical operation that strong edge portion with large weight value and weak edge portion with small weight value. At the phase of kernel estimation, it contains two steps: x and k updating. For the steps x updating, the IFISTA method is used to solve the problem. At the phase of image recovery, we employ non-blind deconvolution to shape the image. What's more, we propose solving it using an efficient alternating minimization method based on a half-quadratic splitting because it contains non-linear penalties for both the data and regularization terms at the phase of image recovery. The experimental results show that we can recover a high-quality reconstructed image.

The road map of this paper is organized as follows: Section II introduces the related works. Section III presents our proposed deblurring algorithm in details. In section IV, the experimental results are detailed. Simultaneously, the proposed algorithm is compared with other algorithms. At finally, we conclude the paper in section V.

II. RELATED WORK

In order to solve the problems of (MAP) formulation. Let x , y and k be the latent image, the given blurred observation and blur kernel, respectively. The deblurring model can be generally represented as:

$$\arg \min_{x,k} \{ \|x \otimes k - B\|_2^2 + \lambda f(x) + \beta f(k)\} \quad (2)$$

where $f(x)$ and $f(k)$ are the prior of latent image x and blur kernel k , respectively. λ and β are the weighting coefficients of $f(x)$ and $f(k)$. To obtain the optimal solution, we can decompose (2) into two sub-problems: x sub-problem and k sub-problem. According to (2), the two sub-problem can be modeled as (3) and (4), respectively.

$$x = \arg \min_x \|x \otimes k - B\|_2^2 + \lambda f(x) \quad (3)$$

$$k = \arg \min_k \|x \otimes k - B\|_2^2 + \beta f(k) \quad (4)$$

The model obviously present that k is the key to get a high quality deblurred image. However, the salient edge and noise suppression are critical for kernel estimation. In recent years, several motion deblurring approaches [21]–[27], [31] have been proposed based on improve edge information.



FIGURE 2. Result of edge extraction, (a) is the strong edge portion, and (b) is the weak edge portion.

Cho and Lee [20] applied the shock filter, which finds the zero-crossing point and then enhances this point according to the magnification of the gradient. Mathematically, the shock filter can be formulated as:

$$I^s = I - \text{sign}(\Delta I) \|\nabla I\| dt \quad (5)$$

Where $\nabla I = \partial_x I^2 * \partial_{xx} I + \partial_x I * \partial_y I * \partial_{xy} I + \partial_y I^2 * \partial_{yy} I$ and $\Delta I = (\partial_x I, \partial_y I)'$ are the Laplacian and gradient of I , respectively. I is the original image. ∂_x , ∂_y , ∂_{xx} , ∂_{yy} and ∂_{xy} are the derivative operators. dt is the time step for a single evolution. Because shock filter is sensitive to noise, it can not only enhance edge information but also enhance noise. Shan *et al.* [8] proposed the idea of using a piecewise function to fit the distribution of the natural image gradient. The algorithm suppressed the ringing phenomenon; however, the computation was still extensive and the running speed was still slow. Zhao *et al.* [32] proposed a method of deblurring an image based on rich edge region extraction using a gray-level co-occurrence matrix. Instead of the entire motion blurred image, the extracted rich edge region is used to estimate the blur kern. Since not all the rich edges region of the image is beneficial to the estimation of the blur kernel, the blur kernel may be not correctly. Moreover, this method ignores the importance of other regional information. Enhance salient image information and noise suppression are always two major parts in image deblurring. In the next section of this literature, we will discuss the solution for the problem in details.

III. PROPOSED METHODOLOGY

Through a large number of experimental studies, we found that Enhance salient image information and noise suppression are critical to obtaining a high quality image. In this paper, the blind deconvolution for image deblurring based on edge enhancement and noise suppression is proposed. The method process can be divided into edge enhancement and noise suppression, blur kernel estimation and blind deconvolution for image deblurring.

A. EDGE ENHANCEMENT AND NOISE SUPPRESSION

In order to better suppress noise, the bilateral filter was often applied to reduce the noise and details from whole image before sharpening the salient edge. After sharpening, the gradient magnitude thresholding is applied to reduce the edges with small gradient. However, some ringing artifacts and noise were not removed because of their large gradient values. Therefore, we proposed trilateral filter method to solve this problem. This literature firstly extracts the strong edge portion.

The classical algorithm of edge detection Sobel is utilized to extract the strong edge information of blurred image. Then, the result image M_s of Sobel detection can be obtained. In M_s , the strong edge was defined as 1, and others were defined as 0. In order to get the strong edge portion x_{se} , we take the inverse operation of the M_s . Therefore, the strong edge portion can be formulated as:

$$x_{se} = M_s * B \quad (6)$$

where B denotes the blurred image. The weak edge portion x_{we} is formulated as:

$$x_{we} = (o_e - M_s) * B \quad (7)$$

where o_e is the matrix that all of elements is 1. FIGURE.2 shows the result of edge extraction.

In this section, the shock filter method was applied to the weak edge portion. According to the formulation (5), we can obtain x^s . Because shock filter is sensitive to noise, the noise of weak edge portion may be enhanced. Consequently, we proposed trilateral filter for x^s to remove noise and enhance edge information. This filter is improved based on bilateral filter. Not only does it suppress impulse noise well, but it also can sharpen image edge information. What's more, the method also can effectively restore images that are contaminated by Gaussian noise and impulse noise

simultaneously. The trilateral filter is formulated as (8).

$$f^t(x_0) = \frac{\sum_{i \in \Omega} w(x_0, y_i) f(y_i)}{\sum_{i \in \Omega} w(x_0, y_i)} \quad (8)$$

Where Ω is a $h \times h$ window centered at the pixel x_0 . $f(y)$ denotes the original image. y_i is the i -th point in Ω . $w(x_0, y)$ is the weight function.

$$w(x_0, y) = w_s(x_0, y) w_r(x_0, y) w_p(x_0, y) \quad y \in \Omega \quad (9)$$

and $y \neq x_0$

$$w_s(x_0, y) = e^{-\frac{|x_0-y|}{2\sigma_s^2}} \quad (10)$$

$$w_r(x_0, y) = e^{-\frac{|f(x_0)-f(y)|}{2\sigma_r^2}} \quad (11)$$

$$w_p(x_0, y) = e^{-\frac{(\sum_{i=1}^m r_i(x_0))^2}{2\sigma_p^2}} \quad (12)$$

where $w_s(x_0, y)$, $w_r(x_0, y)$ and $w_p(x_0, y)$ are Spatial proximity, grayscale similarity and plus weight function, respectively. m is the number of elements in Ω except x_0 . $r_i(x_0) = \{|f(x_0) - f(y)| \mid y \in \Omega \text{ and } y \neq x_0\}$ is the i -th value. If a pixel is an edge point in the image, then at least about half of the points in its neighborhood are similar to their gray values, resulting in a smaller $r(x_0, y)$ value. Otherwise, if the point contaminated by impulse noise, the difference between the other points and the gray value of this point is large, and $r(x_0, y)$ is a relatively large function value. σ_s , σ_r and σ_p are the filter parameters. Substituting (10), (11) and (12) in (9):

$$w(x_0, y) = e^{-\frac{|x_0-y|}{2\sigma_s^2} + \frac{|f(x_0)-f(y)|}{2\sigma_r^2} - \frac{(\sum_{i=1}^m r_i(x_0))^2}{2\sigma_p^2}} \quad (13)$$

In order to reduce the point that is not affected by impulse noise, $w(x_0, y)$ can be re-formulated as:

$$w(x_0, y) = (w_s(x_0, y) w_r(x_0, y))^{1-N(x_0, y)} w_p(x_0, y)^{N(x_0, y)} \quad y \in \Omega \text{ and } y \neq x_0 \quad (14)$$

$N(x_0, y)$ is close to 0 when the image is not contaminated by impulse noise. In contrast, it will be a large value. Therefore, $N(x_0, y)$ can suppress the impulse noise well. $N(x_0, y)$ is defined as:

$$N(x_0, y) = 1 - e^{-\frac{\sum_{i=1}^m r_i(x_0) + \sum_{i=1}^m r_i(y)}{4\sigma_p^2}^2} \quad (15)$$

Finally, we can filter the weak edge portion image based on (8). It can be formulated as:

$$\begin{aligned} x_{we}^t(x) &= \frac{\sum_{i \in \Omega} w(x, y_i) x_{we}(y_i)}{\sum_{i \in \Omega} w(x, y_i)} \\ &= \frac{(o_e - M_s) * \sum_{i \in \Omega} w(x, y_i) B(y_i)}{\sum_{i \in \Omega} w(x, y_i)} \end{aligned} \quad (16)$$

After filtering all pixels of the weak edge image based on (16), the image x_{we}^t can be obtained. Since a salient edge is critical to blur kernel estimation, it is necessary to enhance the image edge information. Therefore, the input image for kernel estimation can be defined as:

$$x' = \xi_1 * x_{we}^t * M_s + \xi_2 * x_{se} \quad (17)$$

Where ξ_1 and ξ_2 are the weight values of strong edge portion and weak edge portion. In (17), the first term suppresses the effect of the trilateral filter on the salient edge. x' can maintain its inherent edge information. According to (6), (7) and (16), x' can be re-formulated as:

$$x' = \left(\frac{(o_e - M_s) * \sum_{i \in \Omega} w(x, y_i) B(y_i)}{\sum_{i \in \Omega} w(x, y_i)} + B \right) * M_s \quad (18)$$

B. KERNEL ESTIMATION

With the image x' , kernel estimation can be accomplished quickly. Most of the energy in images is contained in the low and mid frequency bands, which are barely affected by blur. Therefore, we use discrete filters $\nabla_x = [1, -1]$ and $\nabla_y = [1, -1]^T$ to generate a high-frequency version. We define the objective function with a Gaussian regularization. For kernel estimation, the standard approach to optimizing two sub-problems are to start with an initialization on x and k , and then alternate between x and k updates. For large kernels, an excessive number of x and k updates may be required to converge to a reasonable solution. To mitigate this problem, we perform multiscale estimation of the kernel using a coarse-to-fine pyramid of image resolutions, in a similar manner as in [25]. The x update and k update can be defined with Gaussian regularize. Consequently, the cost function for x update and k update can be modeled as:

$$x = \arg \min_x \|x \otimes k - y\|_2^2 + \lambda \|x\|_2^2 \quad (19)$$

$$k = \arg \min_k \|x \otimes k - y\|_2^2 + \beta \|k\|_2^2 \quad (20)$$

In many situations, it is worthwhile to debias the solution as a post-processing step, to eliminate the attenuation of signal magnitude due to the presence of the regularization term. Therefore, the iterative shrinkage thresholding algorithm (ISTA) was proposed to solve (19) in [21]. Recently, the improved fast iterative shrinkage thresholding algorithm (IFISTA) was also proposed. Comparison the two algorithms, a convergence analysis of the IFISTA algorithm has shown that the IFISTA algorithm has an improved convergence rate as well as an improved restoration capability compared to the ISTA algorithm in [33]. Therefore, we adopt the IFISTA method to solve optimization problem in (19). Algorithm.2 shows the IFISTA algorithm.

where W_n is a positive definite matrix. In order to obtain a stable operation as well as a faster convergence, we propose to use the weighting matrix:

$$W_n = \sum_{j=1}^n \binom{n}{j} (-1)^{j-1} (\mu k^T k)^{j-1} \quad (21)$$

Algorithm 1 Improved Fast Iterative Shrinkage Thresholding Algorithm (IFISTA)

Input: blur kernel k , regularization parameter μ , initial image $x^1 = y$, initial $t_0 = 0$, blur image y , threshold τ , maximum iterations N .

for i=1 to N-1 do

$$\begin{aligned} v &= y - \tau W_n k^T (kx^i - y) \\ x^{i+1} &= S_{\tau\mu}(v) \\ t_i &= \frac{1 + \sqrt{1 + 4t_{i-1}^2}}{2} \\ y &= x^{i+1} + \frac{t_{i-1} - 1}{t_i} (x^{i+1} - x^i) \end{aligned}$$

end for

return output image x^N

In Algorithm.1, S is the soft shrinkage operation on a vector. It shrinks each component of the input vector towards zero:

$$S_\alpha = \max(|x^i| - \alpha, 0) \text{sign}(x^i) \quad (22)$$

As similar as the process of [32], we use the IFISTA step as the inner iteration in our x -update algorithm. The outer loop then simply re-estimates the weighting on the likelihood term in (19) by updating the denominator $\|x\|_2^2$. The overall x update algorithm is as follows:

Algorithm 2 x Update

Input: blur kernel k form k update and image x^1 from x update in Algorithm.1.

Input: maximum outer iterations $M=2$, inner iterations $N=2$.

for j=1 to M-1 do

$$\begin{aligned} \mu &= 1/\lambda_{\max}(k^T k) \\ x^{j+1} &= \text{IFISTA}(k, \mu, x^j, N)(\text{Algorithm.1}) \end{aligned}$$

end for

return update image x^M

In Algorithm.2, k^T is the conjugate transposed matrix of k , $\lambda_{\max}(k^T k)$ denotes the maximum eigenvalue of $k^T k$.

Given the x^M , the blur kernel k can be estimated to solve the k sub-problem. Algorithm 3 outlines our approach for kernel estimation. As the estimation based on gradients has been shown to be more accurate [20]. The minimization problem of k can be rewritten as:

$$k = \arg \min_k \|\nabla x \otimes k - \nabla y\|_2^2 + \beta \|k\|_2^2 \quad (23)$$

where $\nabla = [\nabla_x, \nabla_y]$. (23) is a least squares minimization problem in which a closed-form solution can be computed Fast Fourier transform (FFT). Therefore, the closed-form solution can be written as:

$$k = \mathcal{F}^{-1} \left(\frac{\overline{\mathcal{F}(\nabla_x x)} \mathcal{F}(\nabla_x y) + \overline{\mathcal{F}(\nabla_y x)} \mathcal{F}(\nabla_y y)}{\mathcal{F}(\nabla_x x)^2 + \mathcal{F}(\nabla_y y)^2 + \beta} \right) \quad (24)$$

Where $\mathcal{F}(\cdot)$ and $\mathcal{F}^{-1}(\cdot)$ denote the FFT and inverse FFT respectively. $\mathcal{F}(\cdot)$ is the complex conjugate operator.

Algorithm 3 Kernel Estimation

Input: The image x' which is obtained in section 3.1. Initial kernel k . Build an image pyramid with level index $\{1, 2, \dots, n\}$.

for s=1 to n do

 Resize the image x' with image pyramid

 Compute the high-frequency image x

 for $i = 1$ to m (m is the number of iterations) do

$x^i \leftarrow$ Solving x using Algorithm.2

$k^i \leftarrow$ Update k using (24)

 end for

end for

Output: Kernel estimate k^m

C. IMAGE RECOVERY

Since the blur kernel k has been estimated in previous step. We proposed the non-blind deconvolution to sharp image. Since it contains non-linear penalties for both the data and regularization terms in (3), we propose solving it using an efficient alternating minimization method based on a half-quadratic splitting. In our work, the method proposed by Krishnan *et al.* [34] is preferred, where a hyper-Laplacian prior is used to approximate the distribution of gradients of natural images and avoid the sensitiveness of the estimated kernel. Consequently, the model of image recovery can be formulated as:

$$x = \arg \min_x \|x \otimes k - B\|_2^2 + \lambda \|\nabla x\|_p \quad (25)$$

where $\|\cdot\|_p$ denotes an l_p -norm with $0 < p < 1$. Two auxiliary variables ω_1 and ω_2 are introduced in [35]. The formulation (25) can be written as:

$$\begin{aligned} x = \arg \min_x & \|x \otimes k - B\|_2^2 + \lambda (\|\omega_1\|_p + \|\omega_2\|_p) \\ & + \eta (\|\nabla_x x - \omega_1\|_p + \|\nabla_y x - \omega_2\|_p) \end{aligned} \quad (26)$$

If ω_1 and ω_2 are given, an iterative approach is developed to solve (26). Then, the formulation (26) can be modified as (27). In (26), where η is a control parameter that we will vary during the iteration process.

$$\begin{aligned} x = \arg \min_x & \|x \otimes k - B\|_2^2 \\ & + \eta (\|\nabla_x x - \omega_1\|_p + \|\nabla_y x - \omega_2\|_p) \end{aligned} \quad (27)$$

With the adjusted formulation, (27) can now be solved by an efficient Alternating Minimization (AM) method [35]. This means that we solve $\omega = (\omega_1, \omega_2)$ and x , respectively. First, the initial x is set to the input blurred image B to solve ω problem. Given a fixed x , finding the optimal ω can be simplified into the following optimization problem:

$$\omega = \arg \min_\omega \eta \|\nabla x - \omega\|_2^2 + \lambda \|\omega\|_p \quad (28)$$



FIGURE 3. Deblurred result by our proposed method, (a) Blurred image, (b) Deblurred image, (c) Blur kernel.

To solve the optimization problem of (28), we adopt Krishnan's approach, as detailed in [21]. They numerically solve (28) for all pixels using a lookup table to find ω . After getting ω , the closed form solution of (27) can be written as:

$$x = \mathcal{F}^{-1} \left(\frac{\overline{\mathcal{F}(\nabla_x)}\mathcal{F}(\omega_1) + \overline{\mathcal{F}(\nabla_y)}\mathcal{F}(\omega_2) + \frac{1}{\eta}\overline{\mathcal{F}(k)}\mathcal{F}(B)}{\overline{\mathcal{F}(\nabla_x)}\mathcal{F}(\nabla_x) + \overline{\mathcal{F}(\nabla_y)}\mathcal{F}(\nabla_y) + \frac{1}{\eta}\overline{\mathcal{F}(k)}\mathcal{F}(k)} \right) \quad (29)$$

The nonconvex optimization problem arises from the use of a hyper-Laplacian prior with $p < 1$, then we adopt a splitting approach that allows the non-convexity to become separable over pixels. Algorithm.4 outline the summary of alternating minimization scheme for image recovery.

Algorithm 4 Image Recovery

Input: Blurred image B and the estimated kernel k^m
Initial $x = B$, $\eta = \eta_0$
while (1)
 Solving for ω using (28)
 Solving for x in the frequency domain using (29)
 $\eta \leftarrow \sqrt{2}\eta$
 until $\eta > \eta_{\max}$
Output: Deblurred image x

where η starting with small value we scale it by an integer power until it exceeds some fixed values η_{\max} . At the beginning of each iteration, we first compute ω using (28). Then, given a fixed value of ω , it can minimize (27) to find the optimal x . The iteration process stops when the parameter η is sufficiently large. After the iterative process is completed, we can get the deblurred result. FIGURE.3 shows the deblurred result by our proposed method.

IV. EXPERIMENTS AND DISCUSSION

In this section, we performed several experiments to deblur several examples image. Before image deblurring, the relate parameters should be set about the proposed algorithm. In the majority of deblurring algorithms, parameters setting is

critical to get a high-quality image. Therefore, the correct selection of parameters is required. Based on experience, the filtering effect on impulse noise is better when the two parameters σ_p and σ_j are small in trilateral filter. For better filtering, we adopt a relatively large filtering window. In this literature $\sigma_s = [5 \ 4]^T$, $\sigma_r = [0.8 \ 0.6]^T$, $\sigma_p = [0.3 \ 0.3]^T$ and $\sigma_j = [0.5 \ 0.4]^T$. As similar as [34], our method uses a hyper-Laplacian prior with $p = 2/3$. The η value is varied from 1 to 256 by integer powers of $2\sqrt{2}$. As η is larger than $\eta_{\max} = 256$, the iterations will stop. In (17), ξ_1 and ξ_2 are the weight values of strong edge portion and weak edge portion. Generally, $\xi_1 > 0$, $\xi_2 > 0$, $\xi_1 < \xi_2$ and $1 < \xi_1 + \xi_2 < 2$. In this experiment, we set $\xi_1 = 0.83$, $\xi_2 = 1.15$.

In order to validate our algorithm, we would perform comparison with other well-developed methods. In our experiments, the comparison can be divided into two parts: synthetic image test and real image test. What's more, for testing the visual objective quality, the mean of the peak signal to noise ratio (PSNR) is also used to evaluate quantitatively the deblurred result. Given the blurred image I and unblurred image I^u , the PSNR can be defined as:

$$\text{PSNR} = 10 \cdot \log_{10} \left(\frac{255^2}{\frac{1}{m} \sum_{i=0}^{m-1} \sum_{j=0}^{n-1} [I(i, j) - I^u(i, j)]^2} \right) \quad (30)$$

where $m \times n$ is the size of the input image, $I(i, j)$ is the intensity value of unblurred image and $I^u(i, j)$ is the intensity value of deblurred image.

Synthetic Image Test: We would test the algorithm on the widely used synthetic images from the dataset in Levin *et al.* [26]. This dataset consists of 4 images of size 255×255 and 8 different kernels ranging in size from 13×13 to 27×27 to give a total of 32 blurred images. The few deblurred images with various different methods such as Cho and Lee [20], Shan *et al.* [8] and Xu *et al.* [27] are shown in FIGURE. 4. Based on the image dataset, we then calculate the SSD errors between the deblurred images and the ground truth images. According to Levin *et al.* [26],

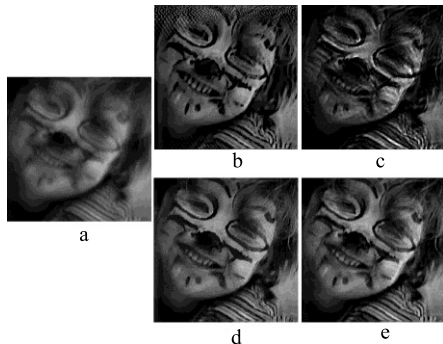


FIGURE 4. Visual deconvolution results by various deconvolution algorithms, (a) Blurred image, (b) Results of Cho&Lee, (c) Results of Shan et al., (d) Results of Xu et al., (e) Results of ours.

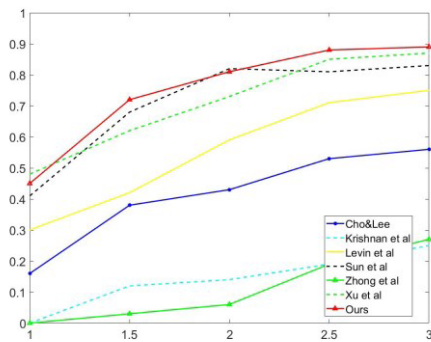


FIGURE 5. Performance comparison using the error ratio measure.

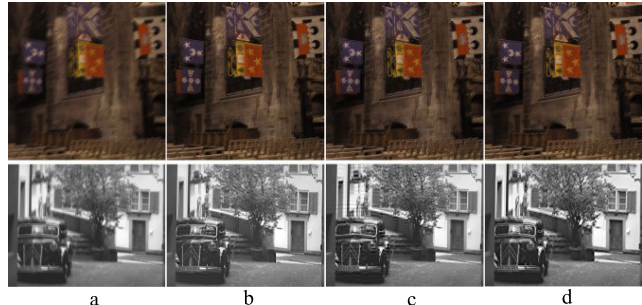


FIGURE 6. More comparisons of synthetic image, (a) blurred image, (b) Results of Hirsch et al. [14], (c) Results of Xu et al. [27], (d) Results of ours.

to normalize the influence of the blur kernel size, we measure the SSD error ratio between deconvolution error with the estimated kernel and deconvolution with the ground truth blur kernel. FIGURE.5 shows the cumulative curves of SSD ratio which include Cho and Lee [20], Krishnan et al. [21], Levin et al. [12], Sun et al. [22], Zhong et al. [3], Xu et al. [27] and the proposed method. As can be seen from FIGURE.5, our method outperforms all competing methods on this test set.

According to the results of the dataset, we compute the mean of structural similarity (SSIM) which was introduced in detail in [26] and PSNR to compare with other methods. TABLE 1 presents the comparison using the image sets which

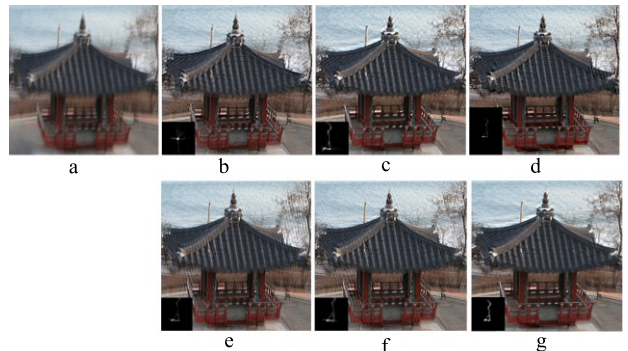


FIGURE 7. Results for restoration of the blurred summerhouse image, (a) is the blurred image, (b)~(g) are the results of Krishnan et al, Levin et al, Cho&Lee, Xu et al, Pan et al and ours, respectively.

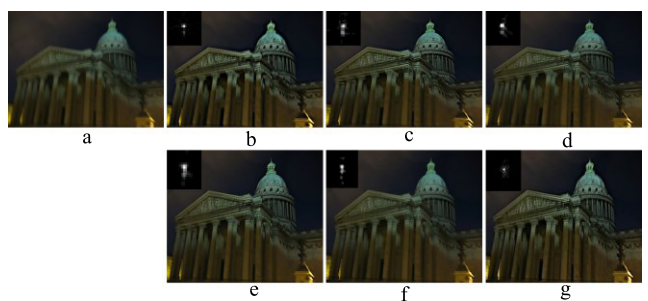


FIGURE 8. Results for restoration of the blurred Pantheon image, (a) is the blurred image, (b)~(g) are the results of Krishnan et al, Cho&Lee, Sun et al, Xu et al, Xu & Jia, and ours, respectively.

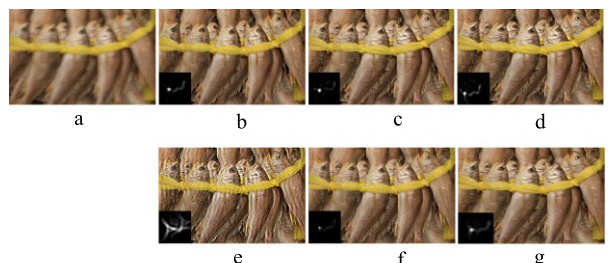


FIGURE 9. Results for restoration of the blurred fishes image, (a) is the blurred image, (b)~(g) are the results of Cho&Lee, Krishnan et al, Levin et al, Pan et al, Sun et al, and ours, respectively.

were used by Levin et al and report the mean PSNR, mean SSIM and geometric mean error ratio for each method. The comparison of all algorithms with the ground-truth shows that our method works better than other algorithms. More comparisons of synthetic image show in FIGURE. 6.

Real Image Test: Next we compare the performance of our algorithm on some real-world examples presented in this paper. Since the ground truth images of the real-world images are un-available, we thus only perform the visual comparison among several sparsity priors based methods. Several real images were used for the comparison. FIGURE.7~FIGURE.9 show the comparison on different real images.

TABLE 1. Quantitative comparison for each method by the dataset in Levin et al.

Methods	PSNR	SSIM	Error Ratio
Known k	33.82	0.93	1.0
Cho&Lee [20]	30.80	0.88	2.01
Krishnan et.al. [21]	24.21	0.76	4.31
Levin et al. [26]	31.14	0.90	1.85
Fergus et al. [25]	29.46	0.85	2.73
Sun et al. [22]	32.38	0.91	1.40
Xu&Jia [31]	28.31	0.87	1.87
Ours	32.65	0.91	1.28

In this literature, the proposed method also adopt non-blind deconvolution for the recovery of real images. As can be seen from the results of FIGURE.6~FIGURE.7, this method can handle image recovery of real images well. Overall our method is robust and generates results that are comparable to, if not better, than the state-of-the-art methods.

V. CONCLUSION

After a majority of experimental researches, we propose a new image deblurring method by edge enhancement and noise suppression. In order to enhance the edge information, the edge detection method is used for separating strong edge portion from images. An improved trilateral filtering is used to suppress the noise and enhance the edge information. The IFISTA method also utilized to estimate blur kernel. Finally, non-blind deconvolution is exploited for image recovery. As future work, we would like to extent our method to handle the blurry image which is blurred or distorted by water waves. In addition, we will also continue to improve the robustness of the algorithm and the quality of deblurred image.

REFERENCES

- [1] D. Gong, R. Li, Y. Zhu, H. Li, J. Sun, and Y. Zhang, "Blind image deblurring by promoting group sparsity," *Neurocomputing*, vol. 310, pp. 190–200, Oct. 2018.
- [2] H. Hong and I. K. Park, "Single-image motion deblurring using adaptive anisotropic regularization," *Opt. Eng.*, vol. 49, no. 9, p. 097008, 2010.
- [3] L. Zhong, S. Cho, D. Metaxas, S. Paris, and J. Wang, "Handling noise in single image deblurring using directional filters," in *Proc. IEEE Conf. Comput. Vis. Pattern Recognit.*, vol. 9, Jun. 2013, pp. 612–619.
- [4] J. Varghese, S. Subash, N. Tairan, and B. Babu, "Laplacian-based frequency domain filter for the restoration of digital images corrupted by periodic noise," *Can. J. Elect. Comput. Eng.*, vol. 39, no. 2, pp. 82–91, 2016.
- [5] H. Hong, X. Hua, T. Zhang, and Y. Shi, "Multi-frame real image restoration based on double loops with alternative maximum likelihood estimation," *Signal Image Video Process.*, vol. 10, no. 8, pp. 1489–1495, Nov. 2016.
- [6] H. Fang, Y. Chang, G. Zhou, and L. Deng, "Iteratively reweighted blind deconvolution with adaptive regularization parameter estimation," *IEEE Access*, vol. 5, pp. 11959–11973, 2017.
- [7] N. Joshi, R. Szeliski, and D. Kriegman, "PSF estimation using sharp edge prediction," in *Proc. IEEE Conf. Comput. Vis. Pattern Recognit. (CVPR)*, Anchorage, AK, USA, Jun. 2008, pp. 1–8.
- [8] Q. Shan, J. Jia, and A. Agarwala, "High-quality motion deblurring from a single image," *ACM Trans. Graph.*, vol. 27, no. 3, p. 73, 2008.
- [9] D. Wipf and H. Zhang, "Revisiting Bayesian blind deconvolution," *J. Mach. Learn. Res.*, vol. 15, no. 1, pp. 3775–3814, 2014.
- [10] Y. Tang, Y. Xue, Y. Chen, and L. Zhou, "Blind deblurring with sparse representation via external patch priors," *Digit. Signal Process.*, vol. 78, pp. 322–331, Jul. 2018.
- [11] R. N. Neelamani, H. Choi, and R. Baraniuk, "ForWaRD: Fourier-wavelet regularized deconvolution for ill-conditioned systems," *IEEE Trans. Signal Process.*, vol. 52, no. 2, pp. 418–433, Feb. 2004.
- [12] A. Levin, Y. Weiss, F. Durand, and W. T. Freeman, "Efficient marginal likelihood optimization in blind deconvolution," in *Proc. IEEE Conf. Comput. Vis. Pattern Recognit. (CVPR)*, Jun. 2011, pp. 2657–2664.
- [13] D. Gong, M. Tan, Y. Zhang, A. van den Hengel, and Q. Shi, "Self-paced kernel estimation for robust blind image deblurring," in *Proc. IEEE Conf. Comput. Vis. Pattern Recognit.*, Oct. 2017, pp. 1670–1679.
- [14] M. Hirsch, C. J. Schuler, S. Harmeling, and B. Schölkopf, "Fast removal of non-uniform camera shake," in *Proc. IEEE Int. Conf. Comput. Vis.*, vol. 23, no. 5, Nov. 2011, pp. 463–470.
- [15] X. Zhou, F. Zhou, and X. Bai, "Blind deconvolution using a nondimensional Gaussianity measure," in *Proc. IEEE Int. Conf. Image Process.*, Sep. 2013, pp. 877–881.
- [16] I. M. El-Henawy, A. A. Ali, K. Ahmed, and H. Adel, "Blind image deblurring using sparse dictionary and orthogonal projections of filtered patches," in *Proc. IEEE Int. Conf. Comput. Eng. Syst.*, Dec. 2015, pp. 274–280.
- [17] J. Kotera, F. Šroubek, and P. Milanfar, "Blind deconvolution using alternating maximum *a posteriori* estimation with heavy-tailed priors," in *Proc. Int. Conf. Comput. Anal. Images Patterns*, 2013, pp. 59–66.
- [18] A. Levin, Y. Weiss, F. Durand, and W. T. Freeman, "Understanding blind deconvolution algorithms," *IEEE Trans. Pattern Anal. Mach. Intell.*, vol. 33, no. 12, pp. 2354–2367, Dec. 2011.
- [19] Y. Wang and W. Yin, "Compressed sensing via iterative support detection," CAAM, Putrajaya, Malaysia, Tech. Rep. TR09-30, 2009.
- [20] S. Cho and S. Lee, "Fast motion deblurring," *ACM Trans. Graph.*, vol. 28, no. 5, p. 145, 2009.
- [21] D. Krishnan, T. Tay, and R. Fergus, "Blind deconvolution using a normalized sparsity measure," in *Proc. IEEE Conf. Comput. Vis. Pattern Recognit. (CVPR)*, Jun. 2011, pp. 233–240.
- [22] L. Sun, S. Cho, J. Wang, and J. Hays, "Edge-based blur kernel estimation using patch priors," in *Proc. IEEE Int. Conf. Comput. Photography (ICCP)*, Apr. 2013, pp. 1–8.
- [23] P. C. Hansen, J. G. Nagy, and D. P. O'Leary, *Deblurring Images: Matrices, Spectra, and Filtering*, Philadelphia, PA, USA: SIAM, 2006.
- [24] A. N. Tikhonov, "Solution of incorrectly formulated problems and the regularization method," *Sov. Math.*, vol. 4, pp. 1035–1038, 1963.
- [25] R. Fergus, B. Singh, A. Hertzmann, S. T. Roweis, and W. T. Freeman, "Removing camera shake from a single photograph," *ACM Trans. Graph.*, vol. 25, no. 3, pp. 787–794, 2006.
- [26] A. Levin, Y. Weiss, F. Durand, and W. T. Freeman, "Understanding and evaluating blind deconvolution algorithms," in *Proc. IEEE Conf. Comput. Vis. Pattern Recognit.*, Jun. 2009, pp. 1964–1971.
- [27] L. Xu, S. Zheng, and J. Jia, "Unnatural L0 sparse representation for natural image deblurring," in *Proc. IEEE Conf. Comput. Vis. Pattern Recognit.*, Jun. 2013, pp. 1107–1114.
- [28] Y. Lou, A. L. Bertozzi, and S. Soatto, "Direct sparse deblurring," *J. Math. Imag. Vis.*, vol. 39, no. 1, pp. 1–12, 2011.
- [29] H. Zhang, J. Yang, Y. Zhang, and T. S. Huang, "Sparse representation based blind image deblurring," in *Proc. IEEE Int. Conf. Multimedia Expo*, Jul. 2011, pp. 1–6.
- [30] J.-F. Cai, H. Ji, C. Liu, and Z. Shen, "Framelet-based blind motion deblurring from a single image," *IEEE Trans. Image Process.*, vol. 21, no. 2, pp. 562–572, Feb. 2012.
- [31] L. Xu and J. Jia, "Two-phase kernel estimation for robust motion deblurring," in *Proc. ECCV*, 2010, pp. 157–170.
- [32] M. Zhao, X. Zhang, Z. Shi, P. Li, and B. Li, "Restoration of motion blurred images based on rich edge region extraction using a gray-level co-occurrence matrix," *IEEE Access*, vol. 6, pp. 15532–15540, 2018.
- [33] M. Z. A. Bhotto, M. O. Ahmad, and M. N. S. Swamy, "An improved fast iterative shrinkage thresholding algorithm for image deblurring," *SIAM J. Imag. Sci.*, vol. 8, no. 3, pp. 1640–1657, 2015.
- [34] D. Krishnan and R. Fergus, "Fast image deconvolution using hyper-laplacian priors," in *Proc. Adv. Neural Inf. Process. Syst.*, 2009, pp. 1033–1041.
- [35] Y. Wang, J. Yang, W. Yin, and Y. Zhang, "A new alternating minimization algorithm for total variation image reconstruction," *SIAM J. Imag. Sci.*, vol. 1, no. 3, pp. 248–272, Aug. 2008.



CHENGTAO CAI received the Ph.D. degree from Harbin Engineering University in 2008, Harbin, China. From 2006 to 2007, he joined the National Research Council, Canada, as a Visiting Scholar. From 2009 to 2011, he was a Post-Doctoral Research Scientist in shipbuilding and oceanography engineering from Harbin Engineering University. His research interests include robot intelligent control and panoramic vision applications.



QIDAN ZHU is currently the Chair of the Intelligent Control Laboratory, College of Automation, Harbin Engineering University. His current research interests are in the area of intelligent control and machine visions.

• • •



HAIYANG MENG is currently pursuing the Ph.D. degree in control science and engineering at the College of Automation, Harbin Engineering University. His research interests include intelligent control, control engineering, and vision sensors.